J Mol Model (2013) 19:4947–4958
DOI 10.1007/s00894-013-1984-8

ORIGINAL PAPER

A DFT study of the Al_2Cl_6-catalyzed Friedel–Crafts acylation of phenyl aromatic compounds

Sigismund T. A. G. Melissen · Vincent Tognetti · Georges Dupas · Julien Jouanneau · Guillaume Lê · Laurent Joubert

Received: 19 June 2013 / Accepted: 22 August 2013 / Published online: 20 September 2013

Abstract The reaction pathways of several Friedel–Crafts acylations involving phenyl aromatic compounds were studied using density functional theory. The reactions were related to the Friedel–Crafts polycondensation of polyaryletherketones. In particular, the acylation of benzene with benzoyl chloride to form benzophenone and variations on this reaction were investigated. The acylation of benzene by one molecule of terephthaloyl chloride or isophthaloyl chloride as well as acylations at the *m*-, *o*-, and *p*-positions of diphenyl ether with one molecule of benzoyl chloride were studied. Adding an additional acyl chloride group to the electrophile appeared to have little influence on the reaction pathway, although the activation energy for the C–C bond-forming steps that occurred when isophthaloyl choride was used was different to the activation energy observed when terephthaloyl chloride was used. Upon changing the nucleophile to diphenyl ether, the reactivity changed according to the trend predicted on based on the *o*-, *p*-directing effects of the ether group. The deprotonation step that restored aromaticity varied widely according to the reaction. The rate-determining step in all of the studied reactions was the formation of the acylium ion, followed in importance by either the formation of the Wheland intermediate or the abstraction of hydrogen, depending on the reactivity of the nucleophile.

Keywords Friedel–Crafts acylation · Density functional theory · Polyaryletherketones · ωb97x-D · Electrophilic aromatic substitution · Stacking

S. T. A. G. Melissen · V. Tognetti · G. Dupas · L. Joubert (✉)
Normandy University, COBRA UMR 6014 & FR 3038, Université de Rouen, INSA Rouen, CNRS, 1 rue Tesniére,
76821 Mont-Saint-Aignan Cedex, France
e-mail: laurent.joubert@univ-rouen.fr

S. T. A. G. Melissen · J. Jouanneau · G. Lê
Arkema CERDATO Laboratories, Route du Rilsan,
27470 Serquigny, France

Introduction

Among the various electrophilic aromatic substitution (EAS) reactions [1] that are described in the literature, the Friedel–Crafts (FC) acylation and alkylation reactions have been among the most important ever since they were first described [2] in 1877, and they have been extensively researched and reviewed [1, 3–5].

FC reactions generally involve the substitution of a hydrogen atom on an aromatic ring by an electrophilic carbon atom. In the case of an FC alkylation, the electrophilic species is generally an alkyl halide. The halogen in this halide is abstracted by a strong Lewis acid (often $FeCl_3$ or $AlCl_3$), forming the reactive carbocation that facilitates the formation of a C–C bond with the aromatic ring. In an FC acylation, the electrophile is an acyl chloride; the Cl^- from this chloride is abstracted with a strong Lewis acid. Superstoichiometric quantities of the Lewis acid are generally added due to the strong oxygen–metal bond that drives the formation of a nonreactive complex.

The strength of the Lewis acid, with $AlCl_3$ being among the strongest known [5], is usually chosen to match the reactivity of the nucleophile. For more reactive heterocyclic aromatics, such as furan, milder Lewis acids such as $ZnCl_2$ can be used.

Spectroscopic studies of the mechanism of the Friedel–Crafts acylation reaction have confirmed the Cl^--abstracting function of the Lewis acid [6] and the existence of the acylium intermediate during the acetylation of benzene [7, 8]; kinetic studies have also confirmed the existence of the Wheland intermediate [9, 10]. Several intermediates have been isolated [11, 12], providing further evidence for the established mechanism.

From a theoretical perspective, numerous investigations of FC acylations have been performed [8, 13–18], including the elucidation of a number of full reaction pathways [19–21]. The interaction of $AlCl_3$ has been found to enhance the nucleophilicity of benzene [13, 14]. The stability of the Al_2Cl_6

dimer with respect to the $AlCl_3$ monomer and its effect on the reaction pathway [15–17] have been investigated, confirming that the former leads to the most favorable reaction pathway and is inherently a more stable species. The NMR properties of several acylium ions [8] were predicted and their existence confirmed. Attempts to elucidate the reaction pathways of several EAS reactions include those for the chlorination of benzene [19], an FC alkylation [20] catalyzed by $AlCl_3$, a carboxylation [21], and a model Al_2Cl_6-catalyzed FC acylation and alkylation [22].

Given the aromatic nature of the nucleophilic species, the selectivity of this reaction has always been a prominent feature of its description [23–26], and appears to be dependent not only on the activation barrier to C–C bond formation but also on the specific geometry of the Wheland intermediate [26–28], which invites an investigation into the complete energetic profiles of these reactions.

Substituents on a phenyl ring give rise to resonance (involving primarily π-bonds) as well as inductive (involving primarily σ-bonds) and steric effects [29], each of which determine the final outcome of the reaction to some extent.

The study described in the present paper was performed to investigate the Friedel–Crafts acylations involved in the synthesis of polyaryletherketones (PAEKs), a family of polymers known for their broad range of applications [30]. These polymers consist of phenylene rings that are connected by ether and ketone groups. The names of these polymers are generally derived from the specific sequence in which the ether (E) and ketone (K) bridges occur, and include such structures as PEK, PEEK, and PEEKK (see Fig. 1 for an example). They can be prepared by the so-called nucleophilic route [31–35] using activated aromatic dihalides and aromatic diphenolates, or the electrophilic route [36–42] via a Friedel–Crafts (FC) polyacylation.

The first successful attempts [36, 37] at the latter route involved the self-condensation of *p*-phenoxybenzoyl chloride in methylene chloride or nitrobenzene to form PEK. Further developments included the polycondensation of diphenyl ether and a mixture of terephthaloyl and isophthaloyl chloride in *o*-dichlorobenzene or 1,2-dichloroethane [38] to form PEKK.

In the present study, the most elementary model FC acylations applicable to PAEK synthesis, i.e., the Al_2Cl_6-catalyzed formation of benzophenone from benzene and benzoyl chloride (BzCl) and derivatives of this reaction were studied using density functional theory (DFT). In particular, the differences in the reactions at the different positions on diphenyl ether (the nucleophile) were investigated, since the occurrence of such side reactions as *ortho*-acylations is well described [23–25]. The use of terephthaloyl and isophthaloyl chloride as electrophiles was explored (see Fig. 1). Calculations were performed primarily in nitrobenzene, focusing exclusively on Al_2Cl_6 as the catalyst species.

Computational details

All calculations were performed with the Gaussian09 quantum chemistry package [43] using the 6-311+G** basis set and the ωB97X-D density functional [44]. This functional is an improvement on the range-separated hybrid functional [45] that employs 100 % Hartree–Fock (HF) exchange for long-range exchange electron–electron interactions and an empirical dispersion correction to account for long-range van der Waals interactions. Hydrogen bonding and stacking can play an important role in the system described, justifying the use of the chosen functional.

A comparison in terms of the obtained geometries and energetics was performed with the B3LYP functional [46–48] because of its widespread popularity [49] and its previous use to describe a similar Friedel–Crafts acylation [22]. It is known [50–52] that B3LYP does not perform well for weak interactions such as hydrogen bonding and stacking [50]. To study the specific contribution of the classical pair-potential dispersion correction, a comparison with the ωB97X [45] functional was also performed.

All structures were optimized in vacuo, and single-point (SP) calculations using the integral equation formalism of the polarized continuum model [53, 54] (IEFPCM) were performed to model the effect of nitrobenzene as solvent. Charge calculations were performed using a natural population analysis [55], which has the advantage of stability for larger basis sets [56]. Intrinsic reaction coordinate (IRC) calculations [57, 58] were performed to check the validity of the reactive pathway that was proposed.

Vibrational analyses were performed on all stationary points at standard ambient temperature and pressure using the harmonic approximation to verify their nature. The calculations yielded one imaginary frequency for each transition state and none for the intermediates, reactants, and products. Calculation of the Gibbs energy in solvent was achieved using the following approximation [59]:

$$\Delta G^0_{\mathrm{solv}} \approx \Delta G^0_{\mathrm{vac}} + \left(E_{\mathrm{SCF,solv}} - E_{\mathrm{SCF,vac}}\right), \quad (1)$$

where ΔG^0 is the Gibbs energy, E_{SCF} is the self-consistent field (SCF) energy of the system, while the subscripts "vac" and "solv" refer to the vacuum and solvent states, respectively.

Results and discussion

Choice of catalyst

To justify the choice of the Al_2Cl_6 dimer as the active catalyst, the Gibbs energy of dimerization of $AlCl_3$ in nitrobenzene was computed and found to be −12.0 kcal/mol^{-1}. The recombination

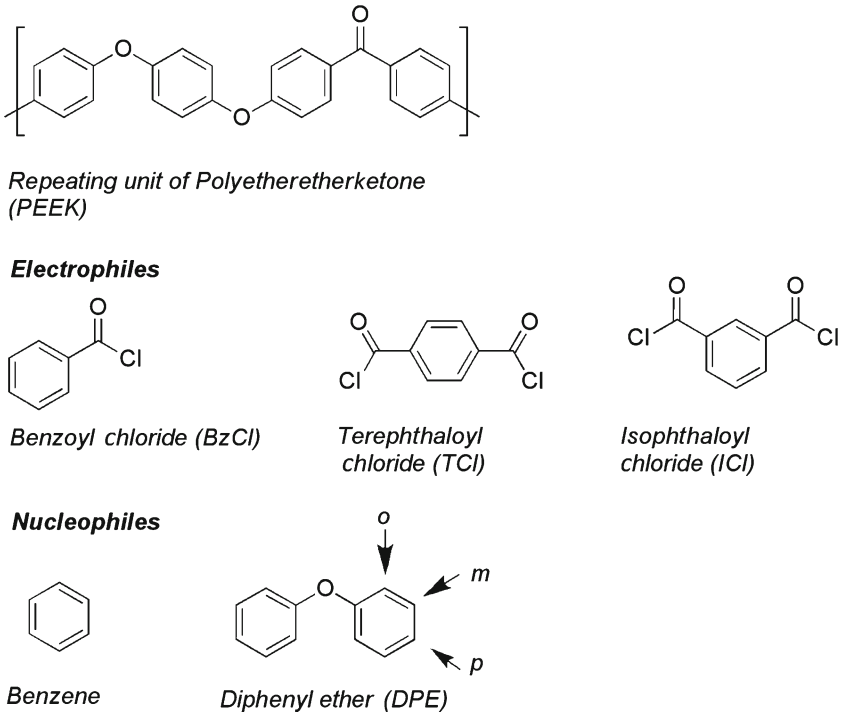

Fig. 1 PEEK, a member of the PAEK polymer family, is shown. Furthermore, the compounds included in our calculations (electrophiles and nucleophiles) are displayed

of $AlCl_3$ and $AlCl_4^-$ to $Al_2Cl_7^-$ was found to be favorable by −9.3 kcal/mol^{-1}, prompting the use of the dimeric form for both the neutral and anionic Al–Cl species.

Reaction between benzene and benzoyl chloride

The first step of the reaction (see Fig. 2 for an overview of the mechanism and Fig. 3 for the optimized structures) is the coordination of Al_2Cl_6 to the oxygen atom of the electrophile to form the precursor complex (Pre), with $d(Al^4–O)$=1.87 Å. Prior to becoming a reactive species, the Al_2Cl_6 dimer undergoes a rearrangement (preceding the abstraction of Cl^- from the nucleophile) through transition state 1 (TS1) to form intermediate 1 (Int1).

Subsequently, the simultaneous dissociation of Al_2Cl_6 from the oxygen atom ($d(Al^4–O)$=2.57 Å) and abstraction of the chlorine atom ($d(Al^4–Cl^3)$=2.51 Å) (TS2) occurs, forming the acylium ion and the $Al_2Cl_7^-$ [Int2A, $d(Al^4–Cl^3$=2.13 Å)] anion. The positive charge of 0.97*e* on the acylium carbon atom (0.97*e* in nitrobenzene) is stabilized by the lone pairs (on chlorine) coordinated to it [$d(Cl^7–C^1)$=3.23 Å, $d(Cl^3–C^1)$= 3.28 Å, $d(Cl^8–C^1)$=3.99 Å], with the charges on the coordinating Cl atoms being −0.54*e* (−0.53*e*), −0.54*e* (−0.53*e*), and −0.51*e* (−0.51*e*), respectively (Fig. 4).

A notable aspect of the obtained geometries is the stacking effect that occurs at the first five stationary points, starting with the precursor, for which $d(C^1–C^{15})$=3.38 Å and ∠(planes)=1.7° (this angle corresponds to the angle between the planes defined by each aromatic group). Stacking is also present in TS2 [$d(C^1–C^{15})$=3.38 Å, ∠(planes)=2.6°] and the π-complex formed [Int2A, d(1,15)=3.22 Å and ∠(planes)=10.2°].

For the reaction to proceed, a σ-complex (Int2B) with $d(C^1,C^{15})$=3.79 Å and ∠(planes)=65.0° must be generated before the C–C bond formation step. The $C^1–C^{15}$ bond (1.96 Å) is then created in the transition state TS3, yielding the Wheland intermediate [Int3, $d(C^1–C^{15})$=1.59 Å]. The positive charge of 0.90*e* (0.92*e*) on the carbocation allows facile re-coordination to the $Al_2Cl_7^-$, which stabilizes it; the anion orients toward the acidic hydrogen atom [$d(H^{21}–Cl^3)$= 2.37 Å, $Q(H^{21})$=0.43*e* (0.42*e*)], which is finally transferred [TS4, $d(H^{21}–Cl^7)$=1.66 Å] to form n intermediate (Int4) in which HCl is coordinated strongly to Al^6. The bond between Cl^5 and Al^4 is slightly weakened (2.42 Å, compared to 2.30 Å in Int3 and 2.34 Å in TS4) to accommodate both bonds.

It is worth mentioning that the existence of two distinct intermediates for FC acylations involving aromatic electrophiles has not yet been described, although the importance of the formation of a reactive intermediate prior to bond formation in EAS reactions has been researched experimentally [60] and computationally [19].

There are major differences between the C–C distances in the transition states for C–C bond formation associated with different Friedel–Crafts type reactions are investigated. For instance, Gothelf [20] obtained a C–C distance of 2.17 Å for a Friedel–Crafts hydroxyalkylation, Yamabe [22] calculated a distance of 1.85 Å in his investigation of FC acylation and 2.08 Å for a similar FC alkylation. The distance of 1.96 Å

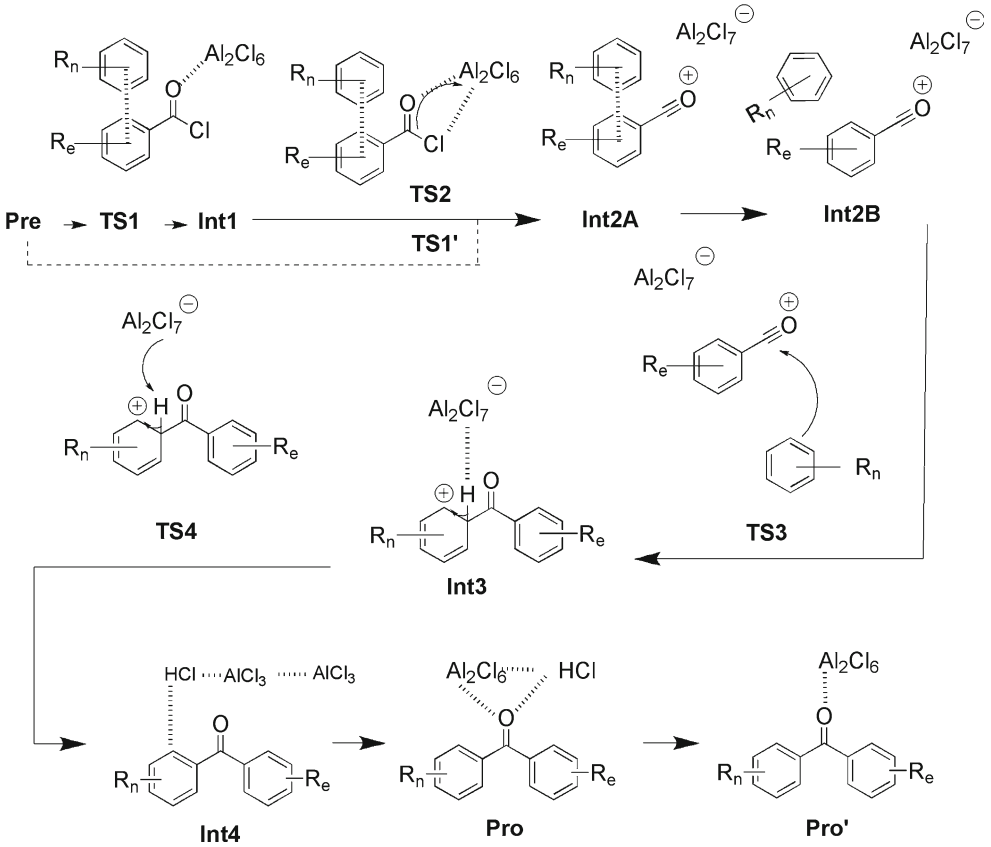

Fig. 2 The general mechanism of the Friedel–Crafts acylation for phenyl aromatic compounds

found here lies between these values. Similar differences were found when comparing the analogs of the C^{15}–H^{21} and Cl^{7}–H^{21} distances for TS4 (1.36 Å and 1.66 Å in this study, respectively). Yamabe [22] determined these distances as 1.45 Å and 1.59 Å, respectively, possibly reflecting the relative stability of the forming benzophenone intermediate; moreover, a hydrogen shift prior to hydrogen abstraction was found in the case of the Friedel–Crafts alkylation reaction.

Subsequently, the product (Pro) with HCl ($d(H^{21}–Cl^{7})$= 1.29 Å) coordinated to the Al_2Cl_6 molecule (through H) is formed with Al^{6}, freed from its coordination with the Cl of HCl, coordinated to the carbonyl group. This "pre-product" leads to the final product (Pro′), from which HCl has been eliminated. The formation of the electrostatically favorable Al–O bond accounts for the large difference in energy between Int4 and Pro, with $Q(Al^{6})$=1.45*e* and $Q(O)$=−0.77*e*, while $d(Al^{6}–O)$=1.82 Å.

Unfortunately, no transition state between Int4 and Pro or between Pro and Pro′ could be identified. It is assumed that, from TS4, there is a complex potential energy surface (PES) with many possible pathways to final HCl dissociation (and many low-energy intermediates), which does not affect the major chemical steps outlined above.

As for the role of solvent, the height of the transition state associated with the Al_2Cl_6 rearrangement (TS1) is 10.7 kcal/mol^{-1} in nitrobenzene and 10.6 kcal/mol^{-1} in vacuo. The abstraction of Cl^{-}, with an activation barrier of 24.1 kcal/mol^{-1} in vacuo and 24.3 kcal/mol^{-1} in nitrobenzene, is the rate-determining step (RDS) of the reaction. Although there is a transition state between the precursor and Int2A (TS1′), the activation energy to form the acylium ion through this TS is 6.0 kcal/mol^{-1} higher than it is through TS2 (6.7 kcal/mol^{-1} in vacuo).

We searched for a transition state between Int2A and Int2B but did not find one. To determine the energy associated with stacking (assuming that a hypothetical transition state between the stacked and unstacked intermediate will probably not exceed the energy of dissociation), separate SP calculations on the benzene ring of Int2A and the "$Al_2Cl_7^{-}$-complexed" acylium ion were performed that revealed a difference in energy of 17.7 kcal/mol^{-1} in vacuo and 14.6 kcal/mol^{-1} in nitrobenzene (with a basis set superposition error of 1.6 kcal/mol^{-1} in vacuo) [61].

The dispersion energies between the aromatic rings in Int2A and Int2B were determined by subtracting the dispersion energies of the individual aromatic rings from the total dispersion energy of the two aromatic rings, yielding −5.6 kcal/mol^{-1} for Int2A and −4.0 kcal/mol^{-1} for Int2B.

Fig. 3 The optimized geometries for the FC acylation of benzene with benzoyl chloride. *Pink* corresponds to aluminum, *green* to chlorine, *red* to oxygen, *white* to hydrogen, and *gray* to carbon

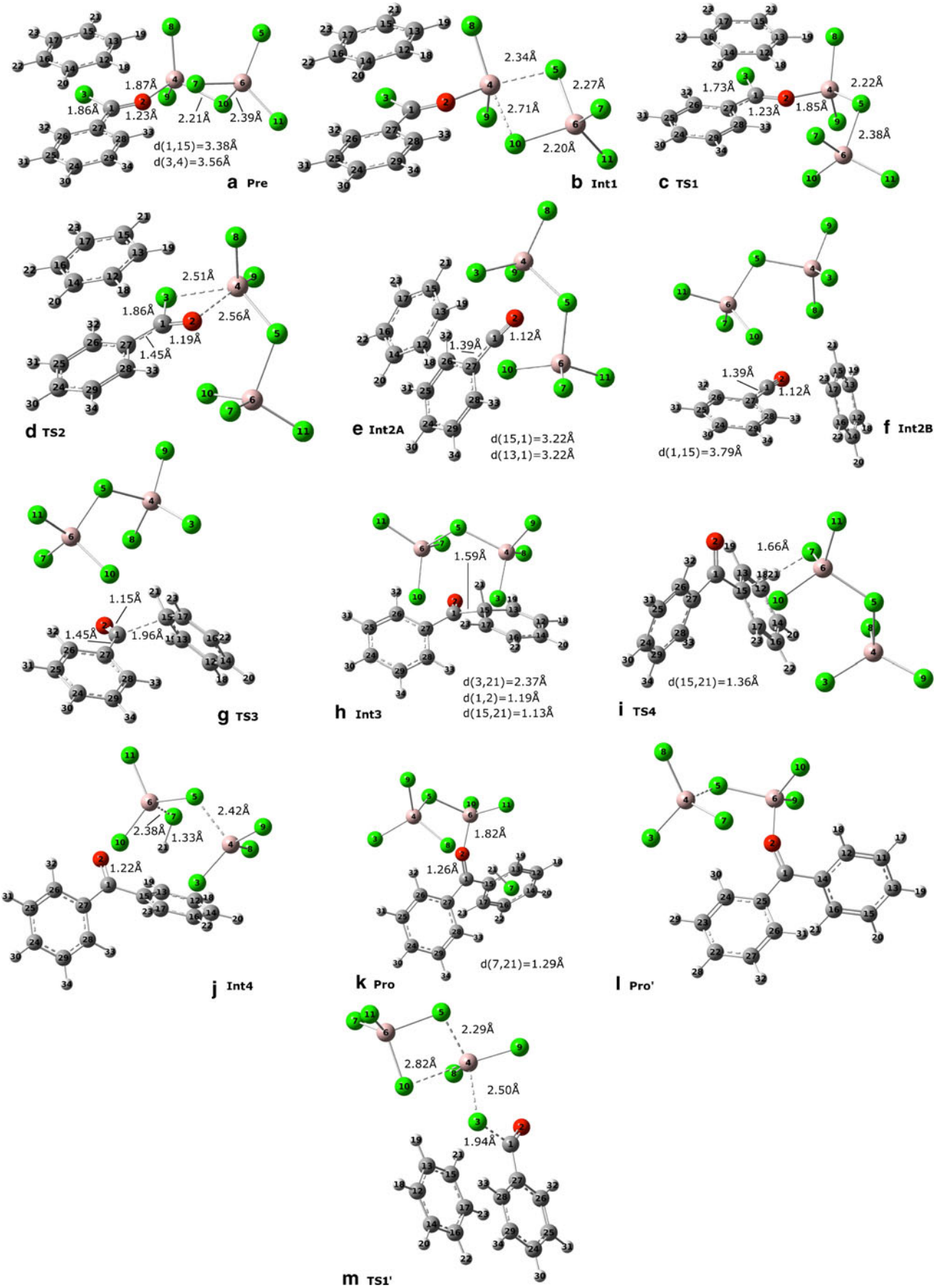
1.87Å
1.86Å
1.23Å
2.21Å
2.39Å
d(1,15)=3.38Å
d(3,4)=3.56Å
a Pre
2.34Å
2.27Å
2.71Å
2.20Å
b Int1
1.73Å
2.22Å
1.23Å
1.85Å
2.38Å
c TS1
2.51Å
1.86Å
2.56Å
1.19Å
1.45Å
d TS2
1.39Å
1.12Å
d(15,1)=3.22Å
d(13,1)=3.22Å
e Int2A
1.39Å
1.12Å
d(1,15)=3.79Å
f Int2B
1.15Å
1.45Å
1.96Å
g TS3
1.59Å
d(3,21)=2.37Å
d(1,2)=1.19Å
d(15,21)=1.13Å
h Int3
1.66Å
d(15,21)=1.36Å
i TS4
2.42Å
2.38Å
1.33Å
1.22Å
j Int4
1.82Å
1.26Å
d(7,21)=1.29Å
k Pro
l Pro'
2.29Å
2.82Å
2.50Å
1.94Å
m TS1'

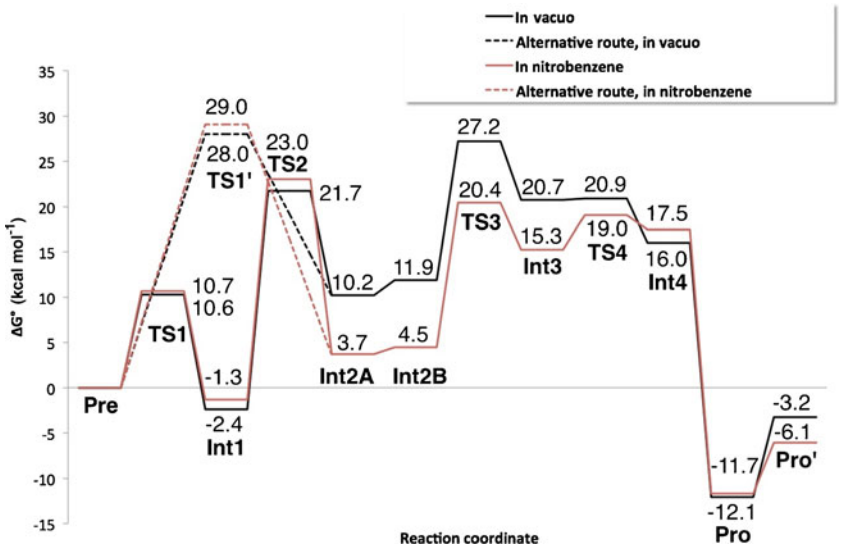

Fig. 4 Gibbs energy profiles of the reaction of benzene with benzoyl chloride in vacuo or in nitrobenzene

Finally, the second most important transition state, TS3, corresponds to an activation barrier of 15.3 kcal/mol^{-1} in vacuo and 15.9 kcal/mol^{-1} in nitrobenzene, compared to 9.9 kcal/mol^{-1} as determined by Yamabe [22], reflecting the relative stability of the benzoylium ion. The least important TS in energetic terms is the abstraction of hydrogen and restoration of aromaticity, TS4, with $\Delta G^{\ddagger}$ equal to 0.1 kcal/mol^{-1} in vacuo and 3.7 kcal/mol^{-1} in nitrobenzene.

Solvent effects

Due to the aromatic nature of both the solvent and the reactants and the possible strong stacking effects between them, we had to check that the implicit description of solvent obtained using structures in vacuo was a sufficiently accurate description of solvent effects.

To this end, Int2B and TS3, the two states determining the activation energy of C–C bond formation, were studied in greater detail. Full geometry optimization of Int2B and TS3 in implicit nitrobenzene yielded a difference in Gibbs energy of 15.9 kcal/mol^{-1}, which is the same as that obtained using our methodology based on a single-point calculation after gas-phase optimization (Eq. 1).

Besides, the inclusion of two benzene molecules (see Fig. 5 and Table 1 for the main energetic and geometric features), one stacking with the nucleophile and the other with the electrophile, was used to determine whether the effect of explicit stacking itself would alter the activation energy. Applying the same method as that used throughout the article, i.e., optimization in vacuo following by an SP calculation in solvent (benzene itself in this particular case), yielded a Gibbs activation energy of 15.1 kcal/mol^{-1}, which is very close to the value obtained without explicit solvent (15.4 kcal/mol^{-1}). A similar calculation with the two benzene molecules mentioned earlier replaced by two nitrobenzene molecules was performed, giving an SCF activation energy of 15.1 kcal/mol^{-1} for this TS3, while the value obtained with Eq. 1 without explicit solvent was 14.9 kcal/mol^{-1}.

The above considerations led us to conclude that the implicit inclusion of the solvent using the PCM model after in vacuo optimization introduced an acceptably small error into the ensuing calculations of the different reactive pathways.

Reaction of diphenyl ether (as the nucleophile) with benzoyl chloride

Upon substituting benzene with diphenyl ether (DPE), the barrier to the abstraction of Cl^{-} is lowered by 0.8 kcal/mol^{-1}, but it remains the RDS (see Fig. 6).

Interestingly, the σ-complexes preceding TS3 lie at higher energies than the π-complexes for *p*-DPE and *m*-DPE, which is also the case for the reaction of benzene, but it is at a lower energy for *o*-DPE due to the absence of steric hindrance between the nonreacting phenoxy group and the benzylium ion (which characterizes the intermediates for *m*-DPE and *p*-DPE). The shortest C–C distance between the nonreacting phenyl group and the benzylium ion are indeed 3.60 Å for *o*-DPE, 4.04 Å for *m*-DPE, and 5.04 Å for *p*-DPE, reflecting the order of the energies of the different intermediates.

Consistent with what is expected based on resonance, the absolute energy of TS3 is 5.8 kcal/mol^{-1} lower for the *p*-position with respect to that for the reaction of benzene with benzoyl chloride; 6.3 kcal/mol^{-1} lower for the *o*-position, but 1.7 kcal/mol^{-1} higher for the most deactivated position, the *m*-position.

When comparing the nucleophilicity on the basis of the activation energy for the formation of the Wheland intermediate, we obtain the following order: *o*-DPE >*p*-DPE >

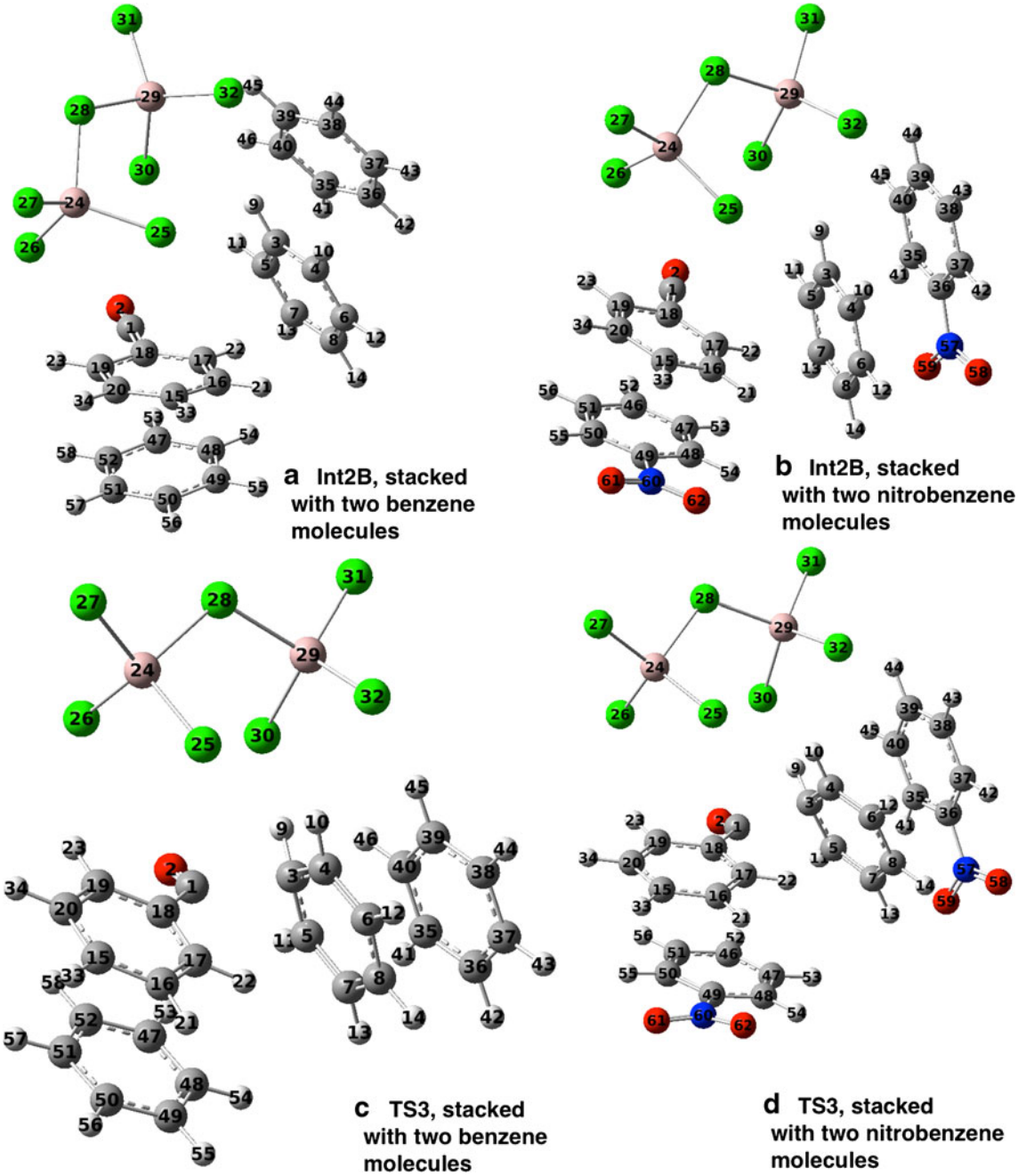

Fig. 5a–d The C–C bond-formation step for the reaction of BzCl with benzene. Views of **a** Int2B stacked with two benzene molecules, **b** Int2B stacked with two nitrobenzene molecules, **c** TS3 stacked with two benzene molecules, **d** TS3 stacked with two nitrobenzene molecules

benzene>*m*-DPE, which is consistent with established linear free-energy relationships [62, 63] for all of the molecules aside from *o*-DPE (the comparison for this molecule is more complicated for steric reasons). That the increase in reactivity upon replacing benzene with the *p*-position of DPE is more dramatic than the decrease in reactivity upon replacing benzene with the *m*-position of DPE is also consistent with these data.

Furthermore, the specific reaction of diphenyl ether with benzoyl chloride using $AlCl_3$ as catalyst has only been described once in the literature [64]; in that work, a low yield (22 %), albeit of the pure *p*-product, was obtained. Research by Sawant et al. [65] on the benzoylation of diphenyl ether using zirconia-supported 12-tungstophosphoric acid as catalyst found product ratios (*p* to *o*) of on the order of 20 or larger (depending on the specific reaction parameters) and no detectable quantities of the *m*-product, giving credence to the C–C bond formation steps analyzed in this manuscript.

Table 1 Comparison of the main geometric and energetic (in kcal/mol^{-1}) features

	Our standard protocol	Optimization employing PCM	Explicit solvent: benzene	Explicit solvent: nitrobenzene
Full optimization	In vacuo	PCM $C_6H_5NO_2$	In vacuo	In vacuo
Subsequent SP calculation (Eq. 1)	PCM $C_6H_5NO_2$	No	PCM C_6H_6	PCM $C_6H_5NO_2$
Explicit solvent	No	No	C_6H_6 (×2)	$C_6H_5NO_2$ (×2)
E^{SCF}(TS3)−E^{SCF}(Int2B)	14.9	15.5	13.4	15.1
ΔG^0(TS3)−ΔG^0(Int2*B*)	15.8	15.9	15.5	–
d(Ar–Ar) in Int2B	4.65	4.71	3.81	4.63
d(Ar–Ar) in TS3	4.49	4.41	4.44	4.43
d(C–C) in Int2B	3.79	4.00	3.26	3.41
d(C–C) in TS3	1.96	2.00	1.98	1.89

A third interesting feature of the reactions of diphenyl ether with BzCl is the differences in the steps that follow TS3. The differences in stability between the Int3 intermediates for *p*-DPE and *o*-DPE on the one hand and *m*-DPE and benzene on the other are also explained by resonance, and reveal an interesting characteristic of this reaction: not only are the activation energies for the formation of the C–C bond lower for *p*-DPE and *o*-DPE, but also, by the same token, the activation energies for deprotonation are higher.

The relevant H–Cl distance in TS4 is 1.66 Å for *p*-DPE, 1.50 Å for *o*-DPE, and 1.49 Å for the *m*-DPE, and these values are qualitatively consistent with the energies associated with dissociation (15.9 kcal/mol^{-1} in the case of *p*-DPE, 18.5 kcal/mol^{-1} in the case of *o*-DPE, and 20.3 kcal/mol^{-1} for *m*-DPE).

For the reaction of BzCl with DPE, the abstraction of Cl^- is still the RDS, but TS4 becomes the second most important step for the *o*- and *p*-positions (13.2 and 16.4 kcal/mol^{-1}, respectively).

Reaction of benzene with iso- and terephthaloyl chloride (as electrophiles)

When studying the reaction of benzene with different phthaloyl chlorides, the most important difference is the decrease in the activation energy of TS3 for ICl by 2.9 kcal/mol^{-1} (see Figs. 7 and 8). It may be that the ICl states that follow the precursor lie are slightly lower in energy than the TCl states due to the fact that the precursor for ICl is destacked whereas the precursor for TCl is stacked (this difference in energy is estimated to be on the order of 1 kcal/mol^{-1}, as that is the difference between the Int1 states for ICl and TCl, whose geometries are very similar and whose phenyl groups are both stacked). Also, the absolute value of TS2 decreases by 1.1 kcal/mol^{-1} for TCl and 0.5 kcal/mol^{-1} for ICl, but it remains the RDS. No equivalent to TS1′ was found for these reactions.

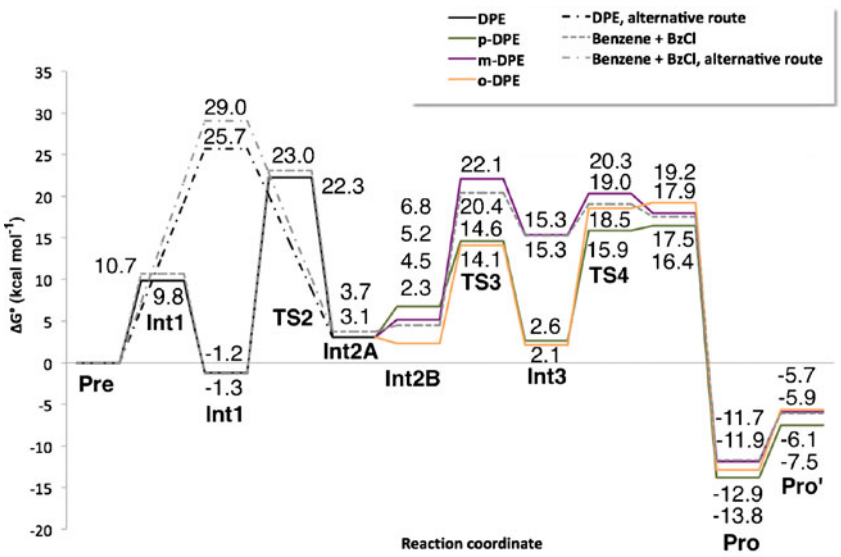

Fig. 6 Gibbs energy profile of the reaction of diphenyl ether (DPE), at the *p*-, *m*-, and *o*-positions, with benzoyl chloride in nitrobenzene

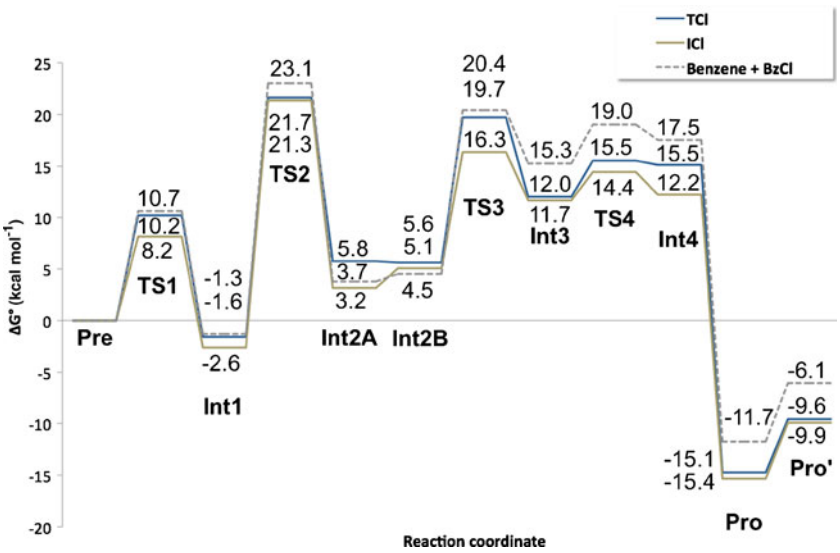

Fig. 7 Gibbs energy profiles for the reaction of benzene with terephthaloyl or isophthaloyl chloride (TCl and ICl) in nitrobenzene

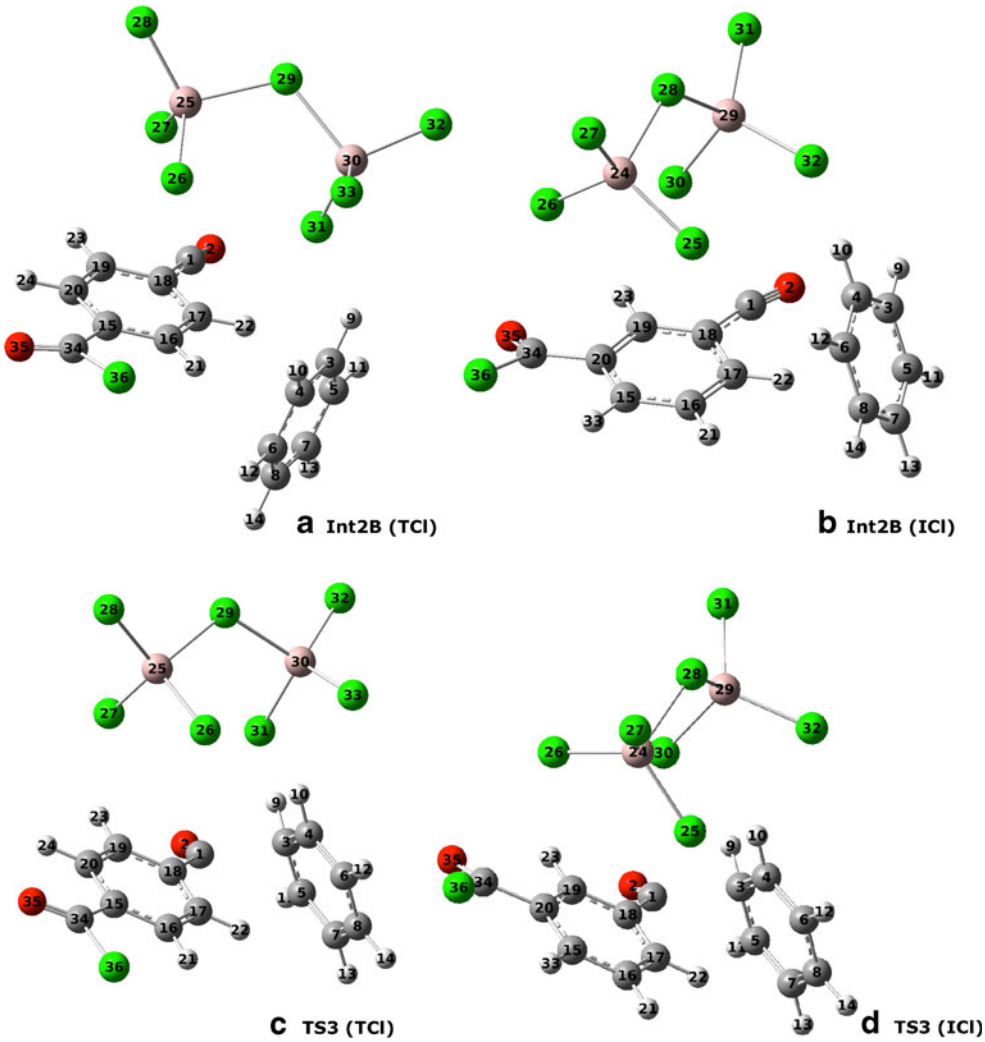

Fig. 8a–d Views of **a** Int2B for TCl with benzene, **b** Int2B for ICl with benzene, **c** TS3 for TCl with benzene, **d** TS3 for ICl with benzene

Comments on the choice of functional and basis set

A comparison between the results obtained using the ωB97X-D, the B3LYP, and the ωB97X (to isolate the effect of the classical dispersion term) functionals was made, considering primarily the stationary states in which stacking plays an important role, and reoptimizing them with the different functionals. Interestingly, Int2A, the intermediate in which the acylium ion is stacked with the benzene, is not found when using B3LYP, its optimization yielding Int2B instead.

Energetically, there are considerable discrepancies between the B3LYP and ωB97X-D results (Int1B: 2.0 kcal/mol^{-1}, TS2: 16.2 kcal/mol^{-1}, Int2B: 11.6 kcal/mol^{-1}), and geometrically there are differences related to the absence of stacking with B3LYP, such as ∠(planes) of 12.7° for Int1B, 17.9° for TS2, and 59.0° for Int2B. The shortest C–C distance in Int1B with B3LYP is 4.01 Å, which should be compared with the value obtained with ωB97X-D (3.29 Å).

The differences between the ωB97X and the ωB97X-D results are subtler. The activation energy associated with TS2 is 24.1 kcal/mol^{-1} with and 23.3 kcal/mol^{-1} without the classical dispersion term. The shortest C–C distance between the electrophile and the nucleophile in Int2A is 3.22 Å with dispersion and 3.25 Å without it. The shortest C–C distance in Int2B both with and without dispersion is 3.48 Å. This is reflected in the increase in energy upon going from the stacked Int2A to the unstacked Int2B, which is 1.6 kcal/mol^{-1} with and 1.0 kcal/mol^{-1} without dispersion. TS3 is 15.3 kcal/mol^{-1} with and 17.7 kcal/mol^{-1} without the pair potential term, which demonstrates that not only the effect of dispersion on the optimized geometry but also the pure dispersion term itself can greatly influence the energetics of the reaction.

To verify that the rather small differences in geometry were consistent with the studied functionals, the parallel-displaced [66] benzene dimer was optimized using both the ωB97X and the ωB97X-D functionals. An SCF dimerization energy of −4.0 kcal/mol^{-1} was found with the D term and −2.3 kcal/mol^{-1} without the D term, and the shortest C–C distance was found to be 3.44 with and 3.54 Å without dispersion. These results show that the long-range scheme allows part of the dispersion to be mimicked. Indeed, B97D does not find a stacked minimum, while ωB97X locates it. This spurious interaction due to exchange is well known for some functionals [67]. It should, however, be added that the direct comparison between ωB97X and ωB97X-D is not as straightforward as it may seem: the exchange-correlation parameters were actually refitted going from ωB97X to ωB97X-D.

Lastly, to verify whether the effect of diffuse functions on the hydrogen atoms has a notable influence on the reaction pathway, Int3, TS4, and Pro were reoptimized, and the Gibbs energy of the barrier to TS4 and the energy difference between TS4 and Pro were determined. Without employing diffuse functions, these values were 0.1 kcal/mol^{-1} and −33.0 kcal/mol^{-1}; when diffuse functions were included, the same steps yielded differences of −0.1 kcal/mol^{-1} and −32.9 kcal/mol^{-1}, respectively, justifying the omission of diffuse functions on the hydrogens.

Conclusions

The Al_2Cl_6-catalyzed Friedel–Crafts acylation of several phenyl aromatic compounds involved in the synthesis of polyaryletherketones was studied, using the reaction of benzene with benzoyl chloride as a starting point for calculations. Iso- and terephthaloyl chloride were used as electrophiles, and the three different reactive positions of diphenyl ether were explored as nucleophiles.

The rate-determining step in this reaction, and the different variations of it that were studied, was the abstraction of chlorine to form the reactive acylium ion ($\Delta G^{\ddagger}$=24.3 kcal/mol^{-1} in nitrobenzene for the reaction of benzene with benzoyl chloride, and between 0.8 and 1.8 kcal/mol^{-1} less for the other reactions), even for the acylation of the DPE *m*-position, the most deactivated nucleophilic position studied. The second most important step was the formation of the Wheland intermediate ($\Delta G^{\ddagger}$=15.9 kcal/mol^{-1} in nitrobenzene) for the reaction of benzene with benzoyl chloride, whereas, for reactions at the *p*- and *o*-positions, the formation of HCl and restoration of aromaticity comprised the second most important step, due to the resonance stabilization of both attacking species as well as the Wheland intermediate itself. Excellent qualitative agreement with experimental data was obtained—the *p*-product is well known to be the major product, followed by the *o*-product (several %), with no detectable amount of *m*-product found in the final product mixture.

In the recently established reactive pathway for the Friedel–Crafts acylation of benzene by acetyl chloride [22], only a single intermediate was found between the transition state forming the acylium ion and the Wheland intermediate. When phenyl aromatic electrophiles such as those studied here are employed, an IRC calculation of the former transition state yields a stacked π-complex, whereas an IRC calculation in the reverse direction of the latter TS yields a reactive σ-complex, showing that the potential energy surface becomes more complex when aromatic electrophiles are involved.

Optimizing the structures in vacuo and then performing an SP calculation in solvent introduces acceptably small errors into both the geometry and the activation energy of the reaction pathway, but allows the performed calculations to be simplified. On the contrary, the use of B3LYP is highly inadvisable.

A remarkable difference of 2.9 kcal/mol^{-1} was obtained between the corresponding C–C bond formation steps in the reactions of isophthaloyl and terephthaloyl chloride.

Our understanding of Friedel–Crafts acylations would be further enhanced by determining whether the reactivities of the molecules involved, particularly the nucleophiles, at the point of C–C bond formation can be determined from the nucleophiles themselves without having to compute the energy of the transition state barrier. A recently developed methodology [68] using the Fukui functions [69] will be used to build on the results of this study.

Acknowledgments The authors would like to acknowledge the Centre de Resources Informatique de Haute-Normandie (CRIHAN), and in particular Dr. P. Bousquet-Melou and Mr. H. Prigent. The authors would like to thank the European Regional Development Fund (ERDF), the Conventions Industrielles de Formation pour la Recherche (CIFRE), the Region Haute-Normandie, and the Arkema group that funded this study.

References

1. Carey FA, Sundberg RJ (2007) Advanced organic chemistry, part A: structure and mechanisms, 5th edn. Springer, New York
2. Friedel C, Crafts JM (1877) Compt Rend 84:1392–1395, 1450–1454
3. Olah GA (1963) Friedel–Crafts and related reactions, vol III, acylation and related reactions. Interscience, New York
4. Eyley SC (1991) Comp Org Synth 2:707–731
5. Heaney H (1991) Comp Org Synth 2:733–752
6. Cassimatis D, Bonnin JP, Theophanides T (1970) Can J Chem 48: 3860–3871. doi:10.1139/v70-650
7. Csihony S, Mehdi H, Homonnay Z, Vértes A, Farkas Ö, Horváth IT (2002) J Chem Soc Dalton Trans 680–685. doi:10.1039/B109303G
8. Xu T, Barich DH, Torres PD, Nicholas JB, Haw JF (1997) J Am Chem Soc 119:396–405. doi:10.1021/ja962944n
9. Olah GA (1971) Acc Chem Res 4:240–248. doi:10.1021/ar50043a002
10. Olah GA, Kobayashi S, Tashiro M (1972) J Am Chem Soc 94:7448–7461. doi:10.1021/ja00776a030
11. Boer FP (1968) J Am Chem Soc 94:6706–6717. doi:10.1021/ja01026a025
12. Chevrier B, Weiss R (1974) Angew Chem 86:12–21. doi:10.1002/ange.19740860103
13. Tarakeshwar P, Lee JY, Kim KS (1998) J Phys Chem A 102:2253–2255. doi:10.1021/jp9807322
14. Tarakeshwar P, Kim KS (1999) J Phys Chem A 103:9116–9124. doi:10.1021/jp992019y
15. Jasien PG (1995) J Phys Chem 99:6502–6508. doi:10.1021/j100017a034
16. Volkov AN, Timoshkin AY, Suvorov AV (2004) Int J Quantum Chem 100:412–418. doi:10.1002/qua.20182
17. Volkov AN, Timoshkin AY, Suvorov AV (2005) Int J Quantum Chem 104:256–260. doi:10.1002/qua.20420
18. Chattaraj PK, Sarkar U, Elango M, Parthasarathi R, Subramanian V (2005) Electrophilicity as a possible descriptor of the kinetic behavior. http://arxiv.org/abs/physics/0509089. Accessed 18 Jan 2013
19. Osamura Y, Terada K, Kobayashi Y, Okazaki R, Ishiyama Y (1999) J Mol Struct THEOCHEM 461–462:399–416. doi:10.1016/S0166-1280(98)00452-7
20. Gothelf AS, Hansen T, Jørgensen KA (2001) J Chem Soc Perkin Trans 1:854–860. doi:10.1039/B009669P
21. Olah GA, Török B, Joschek JP, Bucsi I, Esteves PM, Rasul G, Prakash GKS (2002) J Am Chem Soc 124:11379–11391. doi:10.1021/ja020787o
22. Yamabe S, Yamazaki S (2009) J Phys Org Chem 22:1094–1103. doi:10.1002/poc.1564
23. Olah GA, Moffatt ME, Kuhn SJ, Hardie BA (1964) J Am Chem Soc 86:2198–2202. doi:10.1021/ja01065a019
24. Olah GA, Lukas J, Lukas E (1969) J Am Chem Soc 91:5319–5323. doi:10.1021/ja01047a021
25. Olah GA, Kobayashi S (1971) J Am Chem Soc 93:6964–6967. doi:10.1021/ja00754a045
26. Effenberger F, Maier AH (2001) J Am Chem Soc 123:3429–3433. doi:10.1021/ja0022066
27. Olah GA, Kuhn SJ, Flood SH, Hardie BA (1964) J Am Chem Soc 86: 2203–2209. doi:10.1021/ja01065a020
28. Dowdy D, Gore PH, Waters DN (1991) J Chem Soc Perkin Trans 2: 1149–1159. doi:10.1039/P29910001149
29. Ehrenson S, Brownlee RTC, Taft RW (1973) A generalized treatment of substituent effects in the benzene series. A statistical analysis by the dual substituent parameter equation. In: Streitweiser A Jr, Taft RW (eds) Progress in physical organic chemistry, vol 10. Wiley, New York, pp 1–80
30. Rosato Dominick V, Rosato Donald V, Rosato MV (2004) Plastic product material and process selection handbook. Elsevier, Oxford
31. Salamone JC (ed) (1999) Concise polymeric materials encyclopedia. CRC, Boca Raton
32. Johnson RN, Farnham AG, Clendinning RA, Hale WF, Merriam CN (1967) J Polym Sci A-1 5:2375–2398. doi:10.1002/pol.1967.150050916
33. Attwood TE, Dawson PC, Freeman JL, Hoy LR, Rose JB, Staniland PA (1981) Polymer 22:1096–1103. doi:10.1016/0032-3861(81)90299-8
34. Rose JB, Staniland PA (1982) Thermoplastic aromatic polyetherketones. US Patent 4,320,224
35. Fukawa I, Tanabe T, Dozono T (1991) Macromolecules 24:3838–3844. doi:10.1021/ma00013a016
36. Bonner WH (1962) Aromatic polyketones and preparation thereof. US Patent 3,065,205
37. Goodman I, McIntyre JE, Russel W (1964) Process for the preparation of polymeric ketones. Brit Patent 971,227; Chem Abstr (1964) 61:14805b
38. Brugel E (1991) Stabilization of poly(ether ketone ketones). US Patent 4,987,171
39. Gay FP, Brunette CM (1989) Ordered polyetherketones, US Patent 4,816,556
40. Rueda DR, Zolotukhin MG, Cagiao ME, Ania F, Dosière M, Villers D, de Abajo J (2001) J Macromol Sci B Phys 40:709–731. doi:10.1081/MB-100107557
41. Ueda M, Sato M (1987) Macromolecules 20:2675–2678. doi:10.1021/ma00177a007
42. Zolotukhin MG, Rueda DR, Bruix M, Cagiao ME, Balta Calleja FJ, Bulai A, Gileva NG, Van der Elst L (1997) Polymer 38:3441–3454. doi:10.1016/S0032-3861(96)00909-3
43. Frisch MJ et al. (2009) GAUSSIAN 09. Gaussian, Inc., Wallingford
44. Chai JD, Head-Gordon M (2008) Phys Chem Chem Phys 10:6615–6620. doi:10.1039/B810189B
45. Chai JD, Head-Gordon M (2008) J Chem Phys 128:084106–084121. doi:10.1063/1.2834918
46. Becke AD (1993) J Chem Phys 98:5648–5652. doi:10.1063/1.464913
47. Lee C, Yang W, Parr RG (1988) Phys Rev B 37:785–789. doi:10.1103/PhysRevB.37.785
48. Stephens PJ, Devlin FJ, Chabalowski MJ, Frisch MJ (1994) J Phys Chem 98:11623–11627. doi:10.1021/j100096a001
49. Burke KJ (2012) Chem Phys 136:150901–150908. doi:10.1063/1.4704546
50. Tsuzuki S, Luthi HP (2001) J Chem Phys 114:3949–3957. doi:10.1063/1.1344891
51. Zhao Y, Truhlar DG (2004) J Phys Chem A 108:6908–6918. doi:10.1021/jp048147q
52. Zhao Y, Truhlar DG (2005) J Chem Theory Comput 1:415–432. doi:10.1021/ct049851d
53. Tomasi J, Mennucci B, Cammi R (2005) Chem Rev 105:2999–3094. doi:10.1021/cr9904009

54. Cancès E, Mennucci B, Tomasi J (1997) J Chem Phys 107:3032–3041. doi:10.1063/1.474659
55. Reed AE, Weinstock RB, Weinhold F (1984) J Chem Phys 83:735–746. doi:10.1063/1.449486
56. Politzer P, Mulliken RS (1971) J Chem Phys 55:5135–5137. doi:10.1063/1.1675638
57. Fukui K (1981) Acc Chem Res 14:363–368. doi:10.1021/ar00072a001
58. Gonzalez C, Schlegel HB (1989) J Chem Phys 90:2154–2164. doi:10.1063/1.456010
59. Braga AAC, Ujaque G, Maseras F (2006) Organometallics 25:3647–3658. doi:10.1021/om060380i
60. Fukuzumi S, Kochi JK (1982) J Am Chem Soc 104:7599–7609
61. Boys SF, Bernardi F (1970) Mol Phys 19:553–566. doi:10.1080/00268977000101561
62. McDaniel DH, Brown HC (1958) J Org Chem 23:420–427. doi:10.1021/jo01097a026
63. Stock LM, Brown HC (1963) Adv Phys Org Chem 1:35–154. doi:10.1016/S0065-3160(08)60277-4
64. Brătulescu G (2003) Rev Roum Chim 48:175–177
65. Sawant DP, Devassy BM, Halligudi SB (2004) J Mol Catal Chem 217:211–217. doi:10.1016/j.molcata.2004.03.038
66. Pitoňák M, Neogrády P, Řezáč J, Jurečka P, Urban M, Hobza P (2008) J Chem Theory Comput 4:1829–1834. doi:10.1021/ct800229h
67. Cooper VR (2010) Phys Rev B 81:161104
68. Zielinski F, Tognetti V, Joubert L (2012) Chem Phys Lett 27:67–72. doi:10.1016/j.cplett.2012.01.011
69. Parr RG, Yang W (1984) J Am Chem Soc 106:4049–4050. doi:10.1021/ja00326a036